*Review*

# Modelling the Defect Processes of Materials for Energy Applications

**Efstratia N. Sgourou** [1,2], **Aspassia Daskalopulu** [3], **Ioannis Goulatis** [3], **Yerassimos Panayiotatos** [2], **Andrei L. Solovjov** [4,5], **Ruslan V. Vovk** [5] **and Alexander Chroneos** [3,6,*]

[1] Solid State Physics Section, University of Athens, Panepistimiopolis Zografos, 15784 Athens, Greece
[2] Department of Mechanical Engineering, University of West Attica, 12241 Athens, Greece
[3] Department of Electrical and Computer Engineering, University of Thessaly, 38333 Volos, Greece
[4] B. I. Verkin Institute for Low Temperature Physics and Engineering of National Academy of Science of Ukraine, 47 Nauki Ave., 61103 Kharkov, Ukraine
[5] Department of Physics, V. N. Karazin Kharkiv National University, 4 Svobody Sq., 61077 Kharkiv, Ukraine
[6] Department of Materials, Imperial College London, London SW7 2BP, UK
[*] Correspondence: alexander.chroneos@imperial.ac.uk; Tel.: +30-6978775320

**Abstract:** The technological requirement for ever more efficient materials for the energy and electronics sectors has led to the consideration of numerous compositionally and structurally complicated systems. These systems include solid solutions that are difficult to model using electronic structure calculations because of the numerous possibilities in the arrangement of atoms in supercells. The plethora of such possible arrangements leads to extensive and large numbers of potential supercells, and this renders the investigation of defect properties practically intractable. We consider recent advances in oxide interfaces where studies have demonstrated that it is feasible to tune their defect processes effectively. In this review, we aim to contribute to the ongoing discussion in the community on simple, efficient and tractable ways to realise research in solid solutions and oxide interfaces. The review considers the foundations of relevant thermodynamic models to extract point defect parameters and the special quasirandom structures method to model the supercell of solid solutions. Examples of previous work are given to highlight these methodologies. The review concludes with future directions, systems to be considered and a brief assessment of the relevant methodologies.

**Keywords:** defect engineering; solid solutions; special quasirandom structures; electronic materials; solid oxide fuel cells; nuclear materials

## 1. Introduction

The ever-increasing technological requirements for materials for energy conversion, solar cells, fuel cells, supercapacitors, hydrogen production and nuclear and microelectronic applications [1–20] leads to the consideration of more complicated materials (solid solutions and random alloys) whose properties can be optimised via the tuning of composition and/or external parameters (i.e., strain) [21–30]. It should be noted that the substantial computational resources that have become available in the past few decades have rendered the investigation of the physical and chemical properties of materials using atomistic simulation (for example, using density functional theory (DFT)) an exciting field of research that is complementary to experimental work. Although DFT can offer significant insights into the properties of crystalline materials, it can be difficult and/or time-consuming to apply for solid solutions. This is due to the fact that the replication of the statistics of solid solutions requires the simulation of numerous and very large supercells. This combination of large supercells with the high number of calculations that are required to study defect processes and the impact of all the distinct local environments that will exist into solid solutions renders brute force approaches uneconomical or even practically computationally

intractable [31–35]. In the past few years, there is also an increased application of thermodynamic models (for example, the cBΩ model) that can act in conjunction with experiment and computational modelling to investigate the defect process of solid solutions [36–44].

The first part of the present review focuses on computational ways to model random alloys and solid solutions in an efficient way. The initial part briefly discusses methodologies (special quasirandom structures (SQS), cluster expansion (CE) and thermodynamic models) that are then used to explore the simulation of key paradigms. The second part of the review highlights recent advances in the understanding of oxide interfaces and the ways in which these can be used to tune defect processes.

## 2. Methodology

### 2.1. Thermodynamic Methodology

There have been numerous thermodynamic models aiming to model point defects and their processes in solids, but the $cB\Omega$ model by Varotsos and Alexopoulos is acknowledged as a very efficient and rigorous way to link microscopic and macroscopic properties [36,37,45–51]. The $cB\Omega$ model links the activation Gibbs free energy of a point defect with macroscopic bulk properties of the solid material:

$$g^{act} = c^{act} B \Omega \tag{1}$$

where $B$ is the isothermal bulk modulus, $\Omega$ is the mean atomic volume of the host material and $c^{act}$ is a dimensionless coefficient that is temperature- and pressure-independent.

From Equation (1), it can be derived that the Arrhenius behaviour of the diffusion coefficients for a single diffusion mechanism is:

$$D(T,P) = f g a_0^2 \nu e^{-\frac{c^{act} B \Omega}{k_B T}} \tag{2}$$

where $f$ is the correlation factor, $g$ is a geometrical factor, $a_0$ is the lattice constant, $\nu$ is the attempt frequency and $k_B$ is Boltzmann's constant. Additionally, point defect thermodynamic parameters such as the activation entropy $s^{act}$, activation enthalpy $h^{act}$ and activation volume $v^{act}$ can be deduced via the following relations [37]:

$$s^{act} = -\frac{\partial g^{act}}{\partial T}\Big|_P = -c^{act}\Omega\left\{\frac{\partial B}{\partial T}\Big|_P + \beta B\right\} \tag{3}$$

$$h^{act} = g^{act} + T s^{act} = c^{act}\Omega\left\{B - T\left(\beta B - \frac{\partial B}{\partial T}\Big|_P\right)\right\} \tag{4}$$

$$v^{act} = \frac{\partial g^{act}}{\partial P}\Big|_T = c^{act}\Omega\left\{\frac{\partial B}{\partial P}\Big|_T - 1\right\} \tag{5}$$

where $\beta$ denotes the volumetric coefficient of thermal expansion. These point defect parameters are functions of the elastic and expansion properties of the bulk material.

The $cB\Omega$ model can be employed to self- or hetero-diffusion in the $A_{1-x}B_x$ alloy by considering that the B atoms can be treated as defects [37]. Therefore, the previous relations (Equations (1) and (3)–(5)) can be used to describe the point defect parameters. Henceforth in these expressions, the elastic properties, expansion properties, thermal expansion coefficient and pressure and temperature derivatives will refer to the binary alloy. Therefore, to estimate the defect parameters of $A_{1-x}B_x$, it is imperative to properly determine its bulk properties.

The molar volume of the $A_{1-x}B_x$ alloy with respect to the composition and $T$ (or $P$) is expressed via [37]:

$$V_{A_{1-x}B_x}(x,T) = (1-x)V_A(T) + xV_B(T) \tag{6}$$

where $V_A$ and $V_B$ are the molar volumes of the two end members and $x$ is the molar concentration of component B. It should be stressed that this relation assumes that the

volume change of the alloy obeys Vegard's law (i.e., the volume change of the alloy due to the replacement of atoms A with atoms B does not depend on the concentration $x$). This is a good approximation for a number of systems, but it should be noted that for alloys which strongly deviate from Vegard's law, there should be a third term in Equation (6) representing the deviation from linearity.

Compressibility is defined by $\kappa = 1/B = -\left(\frac{1}{V}\right)(\partial V/\partial P|_T)$. The composition and temperature dependence of the isothermal bulk modulus of $A_{1-x}B_x$ alloy can be derived by differentiating its molar volume (Equation (6)) with respect to $P$ [37]:

$$B_{A_{1-x}B_x}(x, T) = \frac{1 + x(\mu - 1)}{1 + x(\frac{\mu}{\lambda} - 1)} B_A \tag{7}$$

where $\mu = V_B/V_A = \frac{\Omega_B}{\Omega_A}$ is the ratio of the molar volumes or the mean atomic volumes of the end members, whereas $\lambda = B_B/B_A$ is the ratio of their bulk moduli.

Differentiating Equation (7) with respect to $T$ or $P$, we obtain the isobaric temperature derivative $\left(\frac{\partial B_{A_{1-x}B_x}}{\partial T}|_P\right)$ and the isothermal pressure derivative $\left(\frac{\partial B_{A_{1-x}B_x}}{\partial P}|_T\right)$ of the bulk modulus of the alloy:

$$\frac{\partial B_{A_{1-x}B_x}(x)}{\partial T}\Big|_P = \frac{1 + x(\mu-1)}{1 + x(\frac{\mu}{\lambda}-1)} \frac{\partial B_A}{\partial T}\Big|_P$$
$$+ B_A \frac{(1-x)\mu(\beta_{Ge} - \beta_{Si})\left[1 - \frac{x}{\lambda}(1-\mu)\right] - x\frac{\mu}{\lambda}(1-x+x\mu)\left(\frac{1}{B_A}\frac{\partial B_A}{\partial T}|_P - \frac{1}{B_B}\frac{\partial B_B}{\partial T}|_P\right)}{\left(1 - x + x\frac{\mu}{\lambda}\right)^2} \tag{8}$$

and

$$\frac{\partial B_{A_{1-x}B_x}(x)}{\partial P}\Big|_T =$$
$$\frac{1 + x(\mu-1)}{1 + x(\frac{\mu}{\lambda}-1)} \frac{\partial B_A}{\partial P}\Big|_T - x\frac{\mu}{\lambda} \frac{(1-x)(1-\lambda)\left(1 - \frac{1}{\lambda}\right) + (1-x+x\mu)\left(\frac{\partial B_A}{\partial P}|_T - \frac{1}{\lambda}\frac{\partial B_B}{\partial P}|_T\right)}{\left(1 - x + x\frac{\mu}{\lambda}\right)^2} \tag{9}$$

The volumetric coefficient of thermal expansion of the alloy, $\beta_{A_{1-x}B_x}$, is given by [37]:

$$\beta_{A_{1-x}B_x}(x, T) = \beta_A \frac{1 + x(\mu - 1)\left(1 + \frac{\frac{\partial}{\partial T}\left(\frac{\partial B_A}{\partial P}|_T\right)}{\beta_A\left(\frac{\partial B_A}{\partial P}|_T - 1\right)}\right)}{1 + x(\mu - 1)} \tag{10}$$

The $T$ derivative of the quantity $\frac{\partial B}{\partial P}|_T$ in Equation (10) can be estimated through the approximation, $\frac{\partial B/\partial P|_T}{\partial P|_T + 2T\beta\gamma} \approx \partial B^S$, where $B^S$ is the adiabatic bulk modulus and $\gamma$ is the Grüneisen constant [37]. Considering that the T dependencies of $\frac{\partial B^S}{\partial P}$ and $\gamma$ are practically negligible, $\frac{\partial}{\partial T}\left(\frac{\partial B_A}{\partial P}|_T\right)$ can be approximated with $2\gamma\left(\beta + T\left(\frac{\partial \beta}{\partial T}\right)|_P\right)$, which is tractable as it contains terms that can be accessed [37].

These relations provide a way to calculate the elastic and expansion properties, and $c^{act}$ as a function of concentration. At $T = 0$ K, $g^{act}$ is replaced by $h_o^{act}$, and thus, $c^{act}$ is equal to $h_o^{act}/B_o\Omega_o$ [37]. With available experimental diffusion data for a temperature range, the mean value method is also sufficient to calculate $c^{act}$ [50]. Employing Equation (2) in logarithmic form,

$$lnD = lnln\left(fga_0^2\nu\right) - c^{act}\frac{B\Omega}{k_BT} \tag{11}$$

This infers the linear dependence of the experimentally determined $lnD$ with the calculated $\frac{B\Omega}{k_BT}$ using the $cB\Omega$ model for a single diffusion mechanism. Trivially, $c^{act}$ is the slope of the corresponding linear fitting.

### 2.2. Cluster Expansion and Special Quasirandom Structures

Modelling crystal structures using DFT is straightforward from a structural point of view as all that is required is the construction of supercells with periodic boundary conditions. Complications arise when there is structural disorder (i.e., non-stoichiometry and/or atomic species able to occupy multiple crystal sites). Modelling such a system using DFT with the use of large supercells where atoms are randomly inserted in sites can be computationally very expensive, and reproduction of the statistics of the random system may even be practically intractable. Conversely, the SQS approach effectively enables the use of DFT in disordered systems by extracting the physical properties of the random alloy from a small designed cell.

The properties of random alloys (for example, the band gap, total energy and point defect energies) are strongly dependent upon the arrangement of the atoms on the underlying lattice, which is known as configuration $\sigma$. In the cluster expansion (CE) method, the dependence of a given property $f$ on $\sigma$ can be described via [52–58]:

$$f(\sigma) = \sum_{\alpha} D_{\alpha} J_{\alpha} \overline{\Pi}_{\alpha}(\sigma) \tag{12}$$

where $\alpha$ is a figure (cluster) that comprises a group of $k$ lattice sites ($k = 1, 2, 3$ indicates single site, pair, and triplet, and so on), $D_{\alpha}$ is the degeneracy factor that expresses the number of symmetrically equivalent figures of type $\alpha$ per lattice site, $\overline{\Pi}_{\alpha}(\sigma)$ is the correlation function and $J_{\alpha}$ is the effective cluster interaction for figure $\alpha$. When the effective cluster interactions are figured, Equation (12) may be used to extract the properties of any lattice configuration.

Although CE can be deemed as a robust way to characterise the ordered and disordered states within a single framework, the SQS methodology is far more computationally efficient when considering the physical properties of the random alloy. In practice, SQSs are designed small-unit-cell ordered structures that possess correlation functions comparable to the correlation functions of the random alloy [31,59,60]. Since in random alloys there is no pattern in the occupation of the available sites, this results in the alloy correlation functions being expressed as the product of the lattice-averaged spin variables. In a random binary $A_{1-x}B_x$ alloy [58],

$$\left\langle \overline{\Pi}_{\alpha} \right\rangle_R = (2x - 1)^{k_{\alpha}} \tag{13}$$

where $k_{\alpha}$ is the number of vertices in figure $\alpha$. One of the major advantages of the SQS approach in comparison to the CE method is that it can be employed to resolve non-scalar properties such as elastic constants.

Employing periodically repeating supercells may induce erroneous correlations that are not appropriate when modelling a random alloy. The error due to the SQS approximation is [58]:

$$f_{SQS} - \langle f(\sigma) \rangle_R = \sum_{\alpha} D_{\alpha} J_{\alpha} [\left( \overline{\Pi}_{\alpha} \right)_{SQS} - \left\langle \overline{\Pi}_{\alpha} \right\rangle_R] \tag{14}$$

The basic assumption at the heart of the SQS method is that interatomic interactions at large distances are weaker than interactions at smaller distances. This means that the cluster expansion of a property is strongly dependent upon the cluster interactions of the short-ranged clusters. Consequently, it is feasible to form SQSs cells that reproduce the pair and multisite correlation functions of the random alloy between the first few nearest neighbours.

Arguably, more extended SQSs cells can be better because they have smaller periodicity errors and in essence serve as better approximations of the real random alloy. This in turn implies that the predicted physical properties for more extended SQS cells will more accurately match the properties of the random alloy. Nevertheless, it should be noted that in previous investigations for numerous systems, most experimental derived properties rapidly converged with respect to the ones predicted using SQS, with relatively small SQS cells (typically less than 100 atoms) [31,59–63].

## 3. Advanced Materials for Energy Applications

In this section, we will briefly consider the requirements of key energy sectors and their need for advanced materials, with a focus on solid solutions. This is not an exhaustive account but rather aims to introduce the issues. Solid solutions are relevant and under investigation in solid oxide fuel cells, batteries, nuclear fuel, semiconductors, catalysts and superconductors [64–90].

Considering nuclear energy, there is significant research effort for the future generation reactors as nuclear energy is deemed to be an important component of the energy mix aiming to lower $CO_2$ emissions. These advanced nuclear reactors will be required to be safer, more economic and proliferation-resistant. To meet these targets, the community is working on mixed oxide fuels that will be thorium-based due to the abundance of thorium compared to uranium and its highest proliferation resistance [91–95].

There are numerous applications of the SQS and $cB\Omega$ model methodologies in the literature [64–83]. This is driven by the introduction of new material systems and the requirement for easy and inexpensive screening in an effort to lead to application as soon as possible. In that respect, the cBΩ model has been employed to expand our understanding of the defect chemistry of novel microelectronic and nuclear fuel systems.

As expected, most of the studies on nuclear fuel materials from a theoretical perspective focus $UO_2$, but given the requirement for proliferation-resistant fuels (for example, $ThO_2$ and mixed oxides), there are numerous systems and conditions that need to be investigated. Interestingly, in recent studies [40,43,70], there was a combination of molecular dynamics simulations and thermodynamic calculations based on the cBΩ model to consider a wide range of pressures (0–10 GPa), $PuO_2$ and mixed oxide fuels. These studies can serve as a paradigm and a first step for the understanding of these systems, which can be expensive, time-consuming and difficult to study experimentally.

More recently, density functional theory calculations were used in conjunction with the SQS approach to predict the formation of MAX phase solid solutions [90]. MAX phases have a range of ceramic and metallic properties and are thus important candidate materials for numerous applications, including aerospace and nuclear engineering [28–30,75]. Figure 1 illustrates typical 128-atom SQS structures to mimic the $(Zr_{1-x}M_x)_2AlC$ and $Zr_2(Al_{1-x}A_x)C$ MAX phases for x = 0.25 and 0.5 [90]. The results are confirmed by the available experimental data and by employing chemical bonding analysis (crystal-orbital Hamilton population) predict that $(Zr_{1-x}M_x)_2AlC$ (M = Nb, Ta) and $Zr_2(Al_{1-x}A_x)C$ (A = Bi, Pb, Sn) MAX phases can be synthesised [90].

In a further, very significant advancement, Dahlqvist and Rosen [75] performed an extensive (2702 compositions) theoretical study (employing SQS) of MAX phase alloys. This investigation identified as thermodynamically stable 92 i-MAX (in-plane chemical ordering) and 291 solid solution MAX phases [75]. In essence, the study by Dahlqvist and Rosen [75] resulted in a very significant expansion of the MAX phase family and provides promising routes for more focused experimental work. This is illustrated in Figure 2.

The advent of new materials (post-silicon) systems for the new era of nanoelectronics and radiation-tolerant electronic devices has regenerated the interest in the dopant-defect properties and interactions of semiconductor materials (for example, references [26,32–34] and references therein). Materials of interest include the more "classical" systems Ge, $Si_{1-x}Ge_x$ and III–V alloys and the more "modern" systems such as two-dimensional systems including graphene and silicene. For example, Christopoulos et al. [34] employed density function theory and the SQS approach to investigate the effect of electronegativity (of the local environment) on the electronic properties of dopant atoms. It should be stressed that $Si_{1-x}Ge_x$ alloys can be considered as solid solutions as there are two atoms randomly occupying one lattice site (diamond lattice structure). The study by Christopoulos et al. [34] demonstrated that the Bader charge of the dopant atom is highly influenced by the local environment (nearest neighbour), and therefore, dopants may behave differently in areas where there are more Si atoms (Si-rich) compared to areas dominated by Ge atoms (Ge-rich). This is illustrated in Figure 3 for Al-doped $Si_{1-x}Ge_x$ alloys (x = 0.125, 0.25, 0.375, 0.5, 0.625,

0.75 and 0.875), in which there are significant changes in the charge density depending mainly on the composition of the nearest neighbour atoms to the Al substitutional atom.
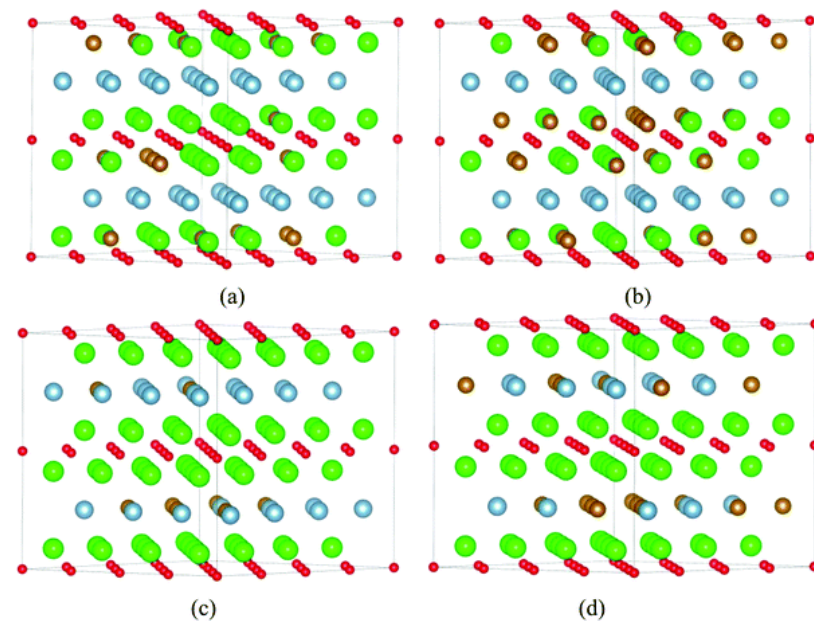


**Figure 1.** 128-atom SQS structures to mimic the $(Zr_{1-x}M_x)_2AlC$ and $Zr_2(Al_{1-x}A_x)C$ MAX phases for x = 0.25 and 0.5 (**a**) $(Zr_{0.75}M_{0.25})_2AlC$, (**b**) $(Zr_{0.5}M_{0.5})_2AlC$, (**c**) $Zr_2(Al_{0.75}A_{0.25})C$, (**d**) $Zr_2(Al_{0.5}A_{0.5})C$. Green spheres represent Zr, whereas blue and red spheres represent Al and C atoms, respectively. Reprinted with permission from the PCCP Owner Societies [90].
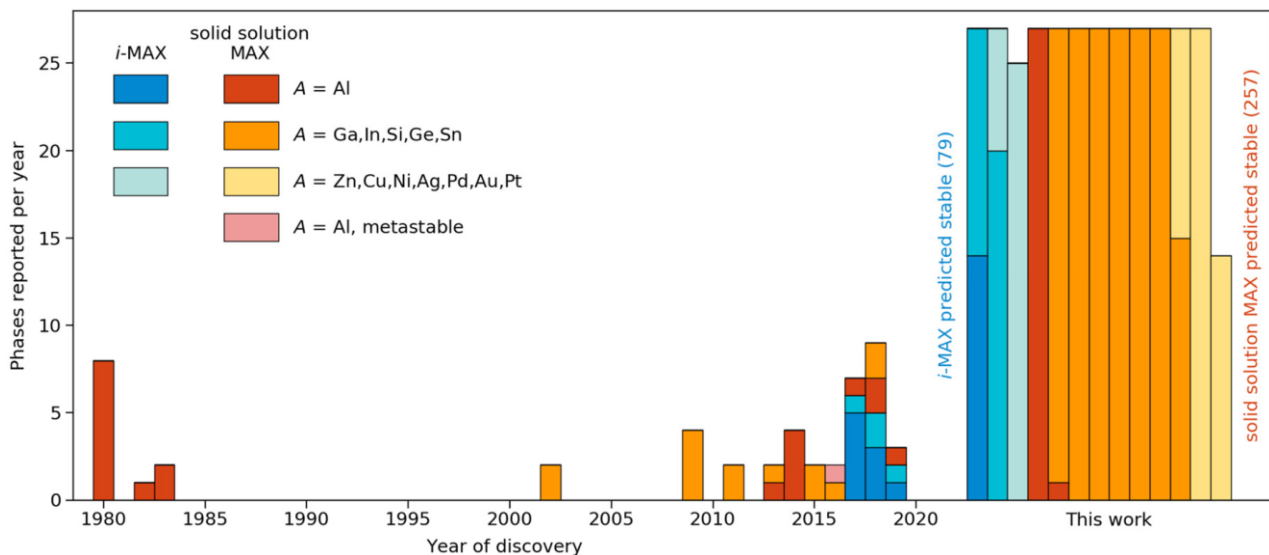


**Figure 2.** Histogram for the experimentally determined theoretically predicted stable MAX phases. The study by Dahlqvist and Rosen (this work has been denoted in the figure) is expected to lead to a significant expansion of the MAX phase compositions. Reproduced from [75] with permission from the Royal Society of Chemistry.
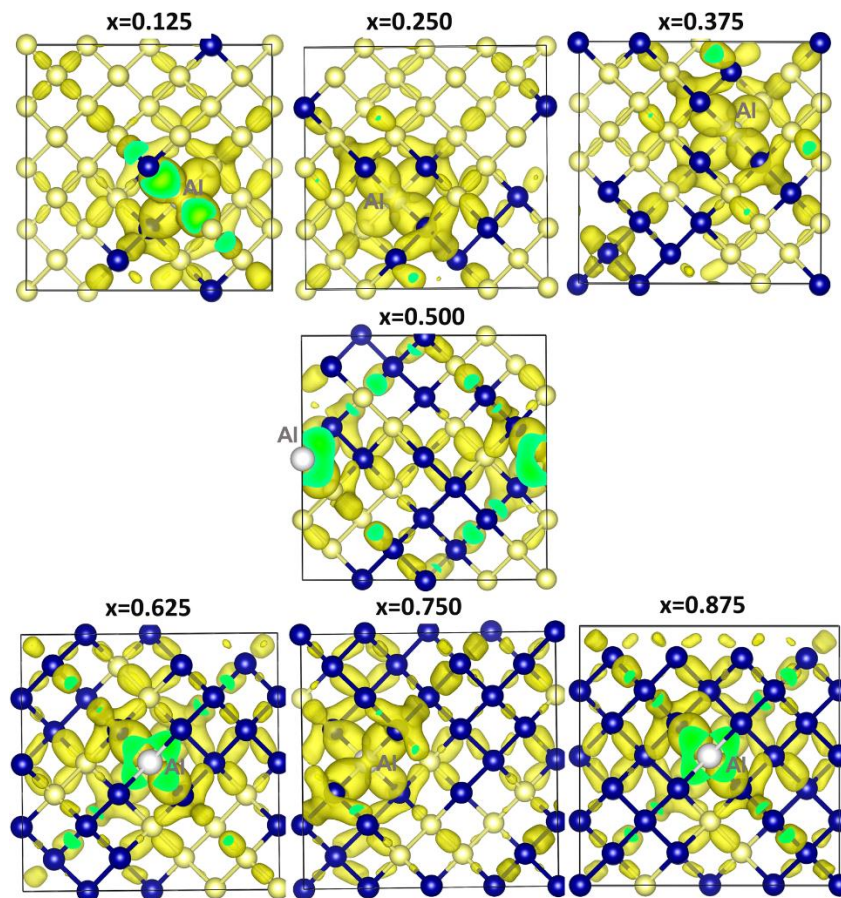
**Figure 3.** Surface of the constant charge density on seven different SQS configurations in $Si_{1-x}Ge_x$ alloys (x = 0.125, 0.25, 0.375, 0.5. 0.625, 0.75 and 0.875) showing the interaction of substitutional Al [34].

## 4. Oxide Interfaces

Nuclear wasteform elements can be encapsulated and immobilised in designed glass–ceramic composites (refer to [58] and references therein). In that respect, understanding the structure–property relations is worthwhile. For these systems, molecular dynamics calculations provide a solid starting point to investigate the impact of the glass–crystal interface on the glass composition [58]. For example, in the study by Rushton et al. (refer to [58] and references therein), molecular dynamics calculations were used to model the interface between MgO and CaO crystals and a mixed alkali borosilicate glass (glass used for the immobilisation of high-level wasteform from the reprocessing of Magnox fuel). A typical system is illustrated in Figure 4 [58]. These studies demonstrated that the crystal remained practically unchanged; however, the glass exhibited considerable structural changes [58]. The alkali concentration increased at the layer closest to the glass–crystal interface, whereas the in the glass network, the crystal induced a partial ordering (with depth up to 10 Å into the glass) [58]. These changes (ordering decreases the entropy in the glass) need to be understood in depth using thermodynamic analysis, and in this respect the cBΩ model may be important.
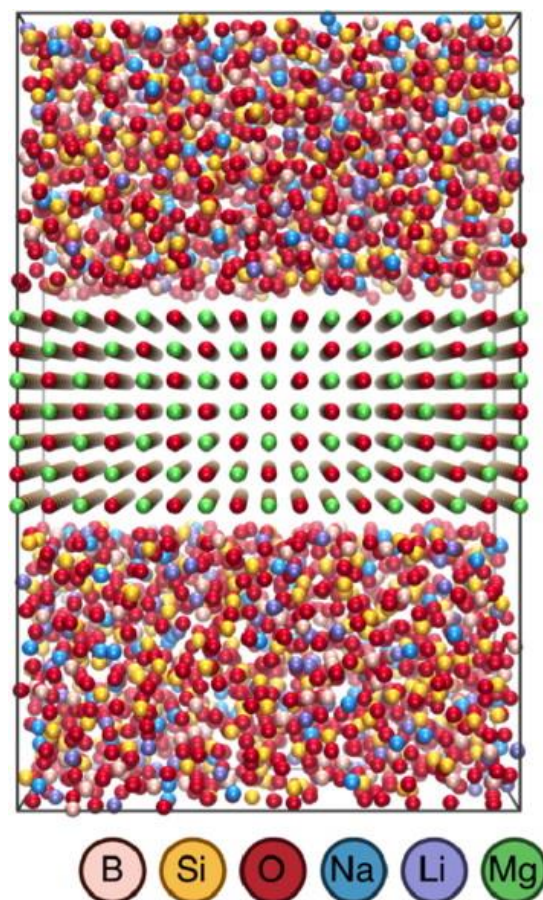
**Figure 4.** Typical model of a glass–crystal interface. The centre is the (1 0 0) surface of MgO and is surrounded by lithium sodium borosilicate glass [58].

Interfaces are also important for energy applications. For example, Garcia-Barriocanal et al. [96] observed colossal conductivity in very thin (~1 nm) yttria-stabilised zirconia (YSZ, here $ZrO_2$ with 8 mol% $Y_2O_3$) layers that were enclosed epitaxially between layers of $SrTiO_3$. These $SrTiO_3/YSZ/SrTiO_3$ heterostructures were determined to have conductivities higher than bulk YSZ by 8 orders of magnitude [96]. They were deemed by Garcia-Barriocanal et al. [96] to be ionic conductivities due to the 7% tensile strain in the YSZ thin films and the disorder of oxygen at the interface. The existence of colossal ionic conductivity can lead to very efficient oxygen-ion conducting electrolytes in solid oxide fuel cells (SOFCs) and in effect has the potential to revolutionise the way we generate and store electricity. The findings of Garcia-Barriocanal et al. [96] have, however, raised a debate in the community about whether the determined conductivity is due to ionic charge carriers (i.e., oxygen diffusion) or electronic charge carriers in the $SrTiO_3$ layers [97–104].

A recent experimental study by Cavallaro et al. [102] in a $SrTiO_3/YSZ/SrTiO_3$ heterostructure determined that the total conductivity dependence is inconsistent with ionic transport in YSZ. Kushima and Yildiz [100] employed DFT in conjunction with the nudged elastic band (NEB) method to calculate the migration enthalpy barrier in biaxially strained bulk YSZ. This study is consistent with an ionic enhancement of up to 4 orders of magnitude. The DFT calculations of Kushima and Yildiz [100] were confined to small supercells at 0 K. Pennycook et al. [103] used quantum molecular dynamics to simulate oxygen-deficient strained $ZrO_2$, calculating a migration energy of 0.4 eV. This was compared with the experimentally determined activation enthalpy for oxygen vacancy migration in unstrained YSZ (refer [96]), resulting in an enhancement in ionic conductivity of $4 \times 10^6$. De Souza et al. [104] criticised the inconsistency of comparing strained $ZrO_2$ with unstrained YSZ and suggested that the enhancement of the ionic conductivity would be far smaller.

That is, considering the experimental migration enthalpies between strained and unstrained YSZ, the enhancement would be less than $4 \times 10^4$.

Recent studies focus on the reduction of the activation enthalpy of oxygen migration and the impact of strain. This is because the enhancement of the ionic conductivity is defined by the ratio of the ionic conductivity in the strained ($\sigma_{ion}$) over the unstrained state ($\sigma_{ion}^0$), given by:

$$\frac{\sigma_{ion}}{\sigma_{ion}^0} \approx exp\left(-\frac{\Delta H_{mig} - \Delta H_{mig}^0}{k_B T}\right) exp\left(\frac{\Delta S_{mig} - \Delta S_{mig}^0}{k_B}\right) \tag{15}$$

where $k_B$ is Boltzmann's constant, $T$ is the temperature, $\Delta H_{mig}$ is the migration enthalpy and $\Delta S_{mig}$ is the migration entropy.

Using Maxwell's relation, the change in the activation entropy of migration $\Delta S_{mig}$ is [104,105]:

$$\frac{\partial \Delta S_{mig}}{\partial p} = -\frac{\partial \Delta V_{mig}}{\partial T} \tag{16}$$

where $p$ is the pressure when there is strain in the film.

The intricacies of oxide interfaces have been thoroughly investigated recently [106–110]. In a recent study, Lee et al. [108] used ionic interfaces to form a non-stoichiometric oxygen vacancy concentration. In particular, the oxide nanobrush architecture they created led to a colossal oxygen vacancy concentration at the fluorite–bixbyite ($CeO_2$-$Y_2O_3$) interface [108]. This is an example of how designed interfacial oxide architectures can in essence tune the formation and transport properties of intrinsic defects that are key for the development of advanced energy technologies.

From a more fundamental material science perspective, the study of Chiabrera et al. [106] determined that tuning the non-stoichiometry in grain boundaries can be used to modify the transport properties. In particular, Chiabrera et al. [106] determined that strain induced defects in the grain boundaries of $La_{1-x}Sr_xMnO_{3\pm\delta}$ (LSM) enhance the oxygen mass transport and abate the electronic and magnetic order. This is consistent with previous work [111–113] but opposite to other oxides in which grain boundaries typically reduce oxygen diffusion [114,115].

The aim of the use of designed interfaces and nanocomposites with complicated architectures and compositions is to be able to tune the physical properties of energy materials and to reduce the use of expensive and scarce materials (for example, rare-earth materials). This can be more difficult in superconducting materials where rare-earth atoms are fundamentally important [116–130].

## 5. Machine Learning Approaches for Defect Prediction

Recent advances in machine learning [131] have been exploited to discover and design of new materials [132] and to solve a large range of predictive problems in materials' defect processes [133,134], which are important for the structural integrity assessment of system components and effective scheduling of maintenance work, in application areas that are safety-critical and require uninterrupted and reliable operation.

Typically, machine learning models are constructed by training them on known datasets, which may include actual or simulated data. The models are subsequently exposed to hitherto unseen (new) data about components that are exposed to conditions similar to those of the training set, and they produce predictions, typically in the form of interpolation or extrapolation depending on the specifics of the application under study.

For instance, Mathew et al. [135] employ neural networks to predict irradiation embrittlement in low-alloy ferritic steel forgings and welds, which are typically used in most reactor pressure vessels of modern light–water nuclear reactors. Irradiation embrittlement causes the formation of many atomic-scale defects within the metal grains and such defects impede the motion of dislocations, leading to an increase in the hardness and a reduction in ductility of steel. Predicting irradiation embrittlement is critical for the safe

and continued operation of the reactor. The research was based on two separate datasets, namely the IVAR data from the Irradiation Variables Experiment [136] and data from the US civil power database (NUREG) [137], which contains the accumulated experience from irradiated surveillance samples from US operators, and built a feed-forward multilayer perceptron (MLP) [138]. The main challenge for irradiation embrittlement forecasting is to establish the correct correlations between the many exposure parameters. Irradiation temperature is one of the most important of these parameters, and although it is feasible to assimilate data on the embrittlement of steels at many temperatures, to predict the actual temperature dependence of embrittlement in a particular steel is hard because of the effect of temperature on other variables such as irradiation flux and the composition of the steel itself. The predictions produced by the ANN that was developed in this study come with high uncertainty; however, once the model is set up, it is relatively easy to retrain it (and improve its performance) as more surveillance data become available.

In a similar spirit, [139] explores the application of probabilistic kernel machines, specifically Gaussian processes, for weld stress prediction, using 16 different kernel functions for prediction. The aim of that work is to produce predictions that would be useful for the a priori scheduling of maintenance for stainless steel pipes, which are critical components for the safe and uninterrupted operation of power plants. Kernel machines are employed in pattern analysis to identify general types of relations (for example, clusters, classifications, principal components) in datasets. The use of kernel functions enables these methods to work in the implicit feature space, without computing the coordinates of data points in that space; hence this "kernel trick" affords cheaper computation. A Gaussian process is a kernel machine with a multivariate normal distribution, and can be seen as the distribution over functions with a continuous domain. The approach was tested using the dataset offered in [140], whose measurements were obtained using various techniques such as deep hole drilling, neutron diffraction and block removal splitting and layering as part of a UK nuclear power industry research programme.

The work in [141] compares different data-driven approaches, specifically artificial neural networks (ANNs) and adaptive neuro-fuzzy inference systems (ANFISs), for the prediction of residual stress in stainless steel welds found in pressure vessels and pipe systems of energy systems. It was established that the application of such data-based models—compared to the finite element approach—is relatively simple and does not require comprehensive information for generating accurate results. The comparison of the approaches was conducted by considering various benchmarks, and ANNs trained using the Levenberg–Marquadt algorithm, and ANFISs based on a hybrid algorithm were found to be better than the ANNs model trained by resilient-backpropagation and ANFISs based on the backpropagation method. However, no single best method emerged from the performance indicators that were considered.

## 6. Summary, Perspective and Future Outlook

In the present review, we considered the modelling of solid solutions and oxide interfaces, which are fundamental to understand in order to optimise them for numerous applications, including nanoelectronics and energy applications such as fuel cells, batteries and nuclear materials. In the examples highlighted here, it is clear that these modelling techniques can (a) be used to further understand defective materials and in a sense aid experimental work (characterisation), (b) lead to the discovery of new solid solution and thus guide the synthesis to the most fruitful systems and (c) result in the fundamental understanding of interfacial properties.

The use of expensive and scarce materials (for example, rare earths or precious metals) in most advanced energy systems needs to be reconsidered so that there is sustainable production. For example, most of the rare earths are mined in China and the local demand will soon outstrip supply. This can lead to a potential reduction in rare-earth exports, which will have a grave impact on a number of industries in numerous countries. Apart from recycling or the discovery and use of more mines, is there a way to move away from the dependence

on scarce materials in advanced energy and nanoelectronic applications? This is a key question that will need to be addressed in the coming years. From the perspective of the present review, it is evident that the manipulation of materials via strained or complicated nanocomposite architectures has the potential to tune materials properties and thus lead to more efficient materials. Manufacturing solutions will play a key role in implementing the required changes and induced complexity at a reasonable cost. In this respect, the fundamental theoretical understanding of materials under strain and at nanocomposite interfaces will become very important. This will require advanced computational techniques based on electronic structure calculations but also thermodynamic modelling. It is anticipated that well-established thermodynamic approaches such as the $cB\Omega$ model can prove to be a valuable ally to atomistic modelling. These models will need to be expanded, though, to account for the intricacies and the complexities of the emerging nanomaterials and their complicated architectures. The technological requirement for advanced materials will need to be addressed in the near future, and advanced designed material configurations could be the way forward to reduce the dependency on rare earths.

The application of artificial intelligence techniques, especially machine learning, could be a promising way to enhance efforts on the design of new materials, on the monitoring of existing infrastructure integrity and on infrastructure degradation forecasting. A critical factor for the successful deployment of such techniques, however, is the availability of appropriate datasets to train the models. Transfer learning, that is, the application of knowledge gained in one domain to a different, but in some ways similar, domain, might be a promising direction to explore, along with the development of more sophisticated cyber-physical systems that can exploit both physical and simulated data.

## References

1. Middleburgh, S.C.; Lumpkin, G.R.; Riley, D. Accommodation, accumulation, and migration of defects in $Ti_3SiC_2$ and $Ti_3AlC_2$ MAX phases. *J. Am. Ceram. Soc.* **2013**, *96*, 3196–3201. [CrossRef]
2. Cooper, M.W.D.; Middleburgh, S.C.; Grimes, R.W. Vacancy mediated cation migration in uranium dioxide: The influence of cluster configuration. *Solid State Ionics* **2014**, *266*, 68–72. [CrossRef]
3. Yang, Y.; Fei, H.; Ruan, G.; Xiang, C.; Tour, J.M. Edge-oriented $MoS_2$ nanoporous films as flexible electrodes for hydrogen evolution reactions and supercapacitor devices. *Adv. Mater.* **2014**, *23*, 8163–8168. [CrossRef] [PubMed]
4. Hadi, M.A.; Vovk, R.V.; Chroneos, A. Physical properties of the recently discovered $Zr_2(Al_{1-x}Bi_x)C$ MAX phases. *J. Mater. Sci. Mater. Electron.* **2016**, *27*, 11925–11933. [CrossRef]
5. Duvel, A.; Heitjans, P.; Fedorov, P.; Scholz, G.; Cibin, G.; Chadwick, A.V.; Pickup, D.M.; Ramos, S.; Sayle, L.W.L.; Sayle, E.K.L.; et al. Is geometric frustration-induced disorder a recipe for high ionic conductivity? *J. Am. Chem. Soc.* **2017**, *139*, 5842–5848. [CrossRef]
6. Yun, S.; Zhou, X.; Even, J.; Hagfeldt, A. Theoretical treatment of $CH_3NH_3PbI_3$ perovskite solar cells. *Angew. Chem.* **2017**, *56*, 15806–15817. [CrossRef] [PubMed]
7. Timerkaeva, D.; Caliste, D.; Deutsch, T.; Pochet, P. Oxygen in silicon: Switch in the diffusion-mediated mechanism. *Phys. Rev. B* **2017**, *96*, 195306. [CrossRef]
8. Dahlqvist, M.; Petruhins, A.; Lu, J.; Hultman, L.; Rosen, J. Origin of chemically ordered atomic laminates (i-MAX): Expanding the elemental space by a theoretical/experimental approach. *ACS Nano* **2018**, *12*, 7761–7770. [CrossRef]
9. Thoda, O.; Xanthopoulou, G.; Vekinis, G.; Chroneos, A. Review of recent studies on solution combustion synthesis of nanostructured catalysts. *Adv. Eng. Mater.* **2018**, *20*, 1800047. [CrossRef]
10. Ning, D.; Baki, A.; Scherb, T.; Song, J.; Fantin, A.; Liu, X.Z.; Schumacher, G.; Banhart, J.; Bouwmeester, H.J.M. Influence of A-site deficiency on structural evolution of $Pr_{2-x}NiO_{4+\delta}$ with temperature. *Solid State Ionics* **2019**, *342*, 115056. [CrossRef]

11. Kuganathan, N.; Iyngaran, P.; Vovk, R.; Chroneos, A. Defects, dopants and Mg diffusion in MgTiO$_3$. *Sci. Rep.* **2019**, *9*, 4394. [CrossRef] [PubMed]

12. Grieshammer, S.; Belova, I.V.; Murch, G.E. Thermodiffusion and ion transport in doped ceria by molecular dynamics simulations. *Acta Mater.* **2021**, *210*, 116802. [CrossRef]

13. Shi, J.; Han, C.; Niu, H.; Zhu, Y.; Yun, S. Theoretical investigation of proton diffusion in Dion-Jacobson layered perovskite RbBiNb$_2$O$_7$. *Nanomaterials.* **2021**, *11*, 1953. [CrossRef] [PubMed]

14. Wang, F.; Xing, Y.; Hu, E.; Wang, J.; Shi, J.; Yun, S.; Zhu, B. PN heterostructure interface-facilitated proton conduction in 3C-SiC/Na$_{0.6}$CoO$_2$ electrolyte for fuel cell application. *ACS Appl. Energy Mater.* **2021**, *4*, 7519–7525. [CrossRef]

15. Igumbor, E.; Olaniyan, O.; Dongho-Nguimbo, G.M.; Mapasha, R.E.; Ahmad, S. Electronic properties and defect levels induced by n/p-type defect complexes in Ge. *Mater. Sci. Semicond. Proc.* **2022**, *150*, 106906. [CrossRef]

16. Pelenitsyn, V.; Korotaev, P. First-principles study of radiation defects in silicon. *Comp. Mater. Sci.* **2022**, *207*, 111273. [CrossRef]

17. Arshad, A.; Yun, S.; Shi, J.; Sun, M.; Zafar, N.; Hagfeldt, A. N-coordinated bimetallic defect-rich nanocarbons as highly efficient electrocatalysts in advanced energy conversion applications. *Chem. Eng. J.* **2022**, *435*, 134913. [CrossRef]

18. Varley, J.B.; Shen, B.; Higashiwaki, M. Wide bandgap semiconductor materials and devices. *J. Appl. Phys.* **2022**, *131*, 230401. [CrossRef]

19. Hassan, J.Z.; Raza, A.; Qumar, U.; Li, G. Recent advances in engineering strategies of Bi-based photocatalysts for environmental remediation. *Sustain. Mater. Technol.* **2022**, *33*, e00478. [CrossRef]

20. Sivaranjani, P.R.; Janani, B.; Thomas, A.M.; Raju, L.L.; Khan, S.S. Recent development in MoS$_2$ based nano-photocatalyst for the degradation of pharmaceutically active compounds. *J. Clean. Prod.* **2022**, *352*, 131506. [CrossRef]

21. Steele, B.C.H. Appraisal of Ce$_{1-y}$Gd$_y$O$_{2-y/2}$ electrolytes for IT-SOFC operation at 500 °C. *Solid State Ionics* **2000**, *129*, 95–110. [CrossRef]

22. Singhal, S.C. Advances in solid oxide fuel cell technology. *Solid State Ionics* **2000**, *135*, 305–313. [CrossRef]

23. Sata, N.; Eberman, K.; Eberl, K.; Maier, J. Mesoscopic fast ion conduction in nanometre scale planar heterostructures. *Nature* **2000**, *408*, 946–949. [CrossRef] [PubMed]

24. Steele, B.C.H.; Heinzel, A. Materials for fuel-cell technologies. *Nature* **2001**, *414*, 345–352. [CrossRef] [PubMed]

25. Jiang, C.; Stanek, C.R.; Sickafus, K.E.; Uberuaga, B.P. First-principles prediction of disordering tendencies in pyrochlore oxides. *Phys. Rev. B* **2009**, *79*, 104203. [CrossRef]

26. Kube, R.; Bracht, H.; Chroneos, A.; Posselt, M.; Schmidt, B. Intrinsic and extrinsic diffusion in germanium. *J. Appl. Phys.* **2009**, *106*, 063534. [CrossRef]

27. Devanathan, R.; Weber, W.J.; Gale, G.D. Radiation tolerance of ceramics- insights from atomistic simulation of damage accumulation in pyrochlores. *Energy Environ. Sci.* **2010**, *3*, 1551–1559. [CrossRef]

28. Horlait, D.; Middleburgh, S.C.; Chroneos, A.; Lee, W.E. Synthesis and DFT investigation of new bismuth-containing MAX phases. *Sci. Rep.* **2016**, *6*, 18829. [CrossRef]

29. Horlait, D.; Grasso, S.; Chroneos, A.; Lee, W.E. Attempts to synthesize quaternary MAX phases (Zr,M)$_2$AlC and Zr$_2$(Al,A)C as a way to approach Zr$_2$AlC. *Mater. Res. Lett.* **2016**, *4*, 137–144. [CrossRef]

30. Zapata-Solvas, E.; Christopoulos, S.R.G.; Ni, N.; Parfitt, D.C.; Horlait, D.; Fitzpatrick, M.E.; Chroneos, A.; Lee, W.E. Experimental synthesis and density functional theory investigation of radiation tolerance of Zr$_3$(Al$_{1-x}$Si$_x$)C$_2$ MAX phases. *J. Am. Ceram. Soc.* **2017**, *100*, 1377–1387. [CrossRef]

31. Zunger, A.; Wei, S.H.; Ferreira, L.G.; Bernard, J.E. Special quasirandom structures. *Phys. Rev. Lett.* **1990**, *65*, 353–356. [CrossRef] [PubMed]

32. Chroneos, A.; Jiang, C.; Grimes, R.W.; Schwingenschlögl, U.; Bracht, H. Defect interactions in Sn$_{1-x}$Ge$_x$ alloys. *Appl. Phys. Lett.* **2009**, *94*, 252104. [CrossRef]

33. Chroneos, A.; Jiang, C.; Grimes, R.W.; Schwingenschlögl, U.; Bracht, H. E centers in Si$_{1-x-y}$Ge$_x$Sn$_y$ alloys. *Appl. Phys. Lett.* **2009**, *95*, 112101. [CrossRef]

34. Christopoulos, S.R.G.; Kuganathan, N.; Chroneos, A. Electronegativity and doping Si$_{1-x}$Gex alloys. *Sci. Rep.* **2020**, *10*, 7459. [CrossRef]

35. Gubaev, K.; Podryabinkin, E.V.; Hart, G.L.W.; Shapeev, A.V. Accelerating high-throughput searches for new alloys with active learning of interatomic potentials. *Comp. Mater. Sci.* **2019**, *156*, 148–156. [CrossRef]

36. Varotsos, P. Calculation of the migration volume of vacancies in ionic solids from macroscopic parameters. *Phys. Stat. Sol.* **1978**, *47*, K133–K136. [CrossRef]

37. Varotsos, P.; Alexopoulos, K. *Thermodynamics of Point Defects and Their Relation with the Bulk Properties*; Elsevier: Amsterdam, The Netherlands, 1986.

38. Zhang, B.; Wu, X.; Xu, J.; Zhou, R. Application of the cBΩ model for the calculation of oxygen self-diffusion coefficients in minerals. *J. Appl. Phys.* **2010**, *108*, 053505. [CrossRef]

39. Vallianatos, F.; Saltas, V. Application of the *cBΩ* model to the calculation of diffusion parameters of He in olivine. *Phys. Chem. Miner.* **2014**, *41*, 181–188. [CrossRef]

40. Cooper, M.W.D.; Grimes, R.W.; Fitzpatrick, M.E.; Chroneos, A. Modeling oxygen self-diffusion in UO$_2$ under pressure. *Solid State Ionics* **2015**, *282*, 26–30. [CrossRef]

41. Zhang, B.; Shan, S. Application of the *cBΩ* model to the calculation of diffusion parameters of Si in silicates. *Geochem. Geophys. Geosyst.* **2015**, *16*, 705–718. [CrossRef]

42. Chroneos, A.; Vovk, R.V. Modeling self-diffusion in $UO_2$ and $ThO_2$ by connecting point defect parameters with bulk properties. *Solid State Ionics* **2015**, *274*, 1–3. [CrossRef]

43. Parfitt, D.C.; Cooper, M.W.D.; Rushton, M.J.D.; Christopoulos, S.-R.G.; Fitzpatrick, M.E.; Chroneos, A. Thermodynamic calculations of oxygen self-diffusion in mixed-oxide nuclear fuels. *RSC Adv.* **2016**, *6*, 74018–74028. [CrossRef]

44. Saltas, V.; Chroneos, A.; Vallianatos, F.A. A thermodynamic approach of self- and hetero-diffusion in GaAs: Connecting point defect parameters with bulk properties. *RSC Adv.* **2016**, *6*, 53324–53330. [CrossRef]

45. Varotsos, P. Comparison of models that interconnect point defect parameters in solids with bulk properties. *J. Appl. Phys.* **2007**, *101*, 123503. [CrossRef]

46. Varotsos, P. Point defect parameters in β-$PbF_2$ revisited. *Solid State Ionics* **2008**, *179*, 438–441. [CrossRef]

47. Chroneos, A. Connecting point defect parameters with bulk properties to describe diffusion in solids. *Appl. Phys. Rev.* **2016**, *3*, 041304. [CrossRef]

48. Saltas, V.; Chroneos, A.; Vallianatos, F.A. A thermodynamic approach to self-diffusion in silicon: Evidence of a single diffusion mechanism? *Mater. Chem. Phys.* **2016**, *181*, 204–208. [CrossRef]

49. Sarlis, N.V.; Skordas, E.S. Estimating the compressibility of osmium from recent measurements of Ir-Os alloys under high pressure. *J. Phys. Chem. A* **2016**, *120*, 1601–1604. [CrossRef]

50. Saltas, V.; Chroneos, A.; Vallianatos, F.A. Composition and temperature dependence of self-diffusion in $Si_{1-x}Ge_x$ alloys. *Sci. Rep.* **2017**, *7*, 1374. [CrossRef] [PubMed]

51. Skordas, E.S.; Sarlis, N.V.; Varotsos, P.A. Applying the cBΩ thermodynamical model to LiF using its equation of state obtained from high pressure diamond anvil cell measurements. *Solid State Ionics* **2020**, *354*, 115404. [CrossRef]

52. Connolly, J.W.D.; Williams, A.R. Density functional theory applied to phase transformations in transition metal alloys. *Phys. Rev. B* **1983**, *27*, 5169–5172. [CrossRef]

53. Sanchez, J.M.; Ducastelle, F.; Gratias, D. Generalized cluster description of multicomponent systems. *Physica A* **1984**, *128*, 334–350. [CrossRef]

54. Laks, D.B.; Ferreira, L.G.; Froyen, S.; Zunger, A. Efficient cluster expansion for substitutional systems. *Phys. Rev. B* **1992**, *46*, 12587–12605. [CrossRef]

55. Wolverton, C.; Zunger, A. Ising-like description of structurally released ordered and disordered alloys. *Phys. Rev. Lett.* **1995**, *75*, 3162–3165. [CrossRef]

56. Zunger, A.; Wang, L.G.; Hart, G.L.W.; Sanati, M. Obtaining Ising-like expansions for binary alloys from first principles. *Model. Simul. Mater. Sci. Eng.* **2002**, *10*, 685–706. [CrossRef]

57. Jiang, C.; Sordelet, D.J.; Gleeson, B. First-principles study of phase stability in pseudobinary $(Ni_{1-x}Pt_x)_3Al$. *Phys. Rev. B* **2005**, *72*, 184203. [CrossRef]

58. Chroneos, A.; Rushton, M.J.D.; Jiang, C.; Tsoukalas, L.H. Nuclear wasteform materials: Atomistic simulation case studies. *J. Nucl. Mater.* **2013**, *441*, 29–39. [CrossRef]

59. Wei, S.H.; Ferreira, L.G.; Bernard, J.E.; Zunger, A. Electronic properties of random alloys: Special quasirandom structures. *Phys. Rev. B* **1990**, *42*, 9622–9649. [CrossRef] [PubMed]

60. Jiang, C.; Wolverton, C.; Sofo, J.; Chen, L.Q.; Liu, Z.K. First-principles study of binary bcc alloys using special quasirandom structures. *Phys. Rev. B* **2004**, *69*, 214202. [CrossRef]

61. Murphy, S.T.; Chroneos, A.; Jiang, C.; Schwingenschlögl, U.; Grimes, R.W. Deviations from Vegard's law in ternary III-V alloys. *Phys. Rev. B* **2010**, *82*, 073201. [CrossRef]

62. Murphy, S.T.; Chroneos, A.; Grimes, R.W.; Jiang, C.; Schwingenschlögl, U. Phase stability and the arsenic vacancy defect in $In_xGa_{1-x}As$. *Phys. Rev. B* **2011**, *84*, 184108. [CrossRef]

63. Wang, H.; Chroneos, A.; Jiang, C.; Schwingenschlögl, U. Modelling zirconium hydrides using the special quasirandom structure approach. *Phys. Chem. Chem. Phys.* **2013**, *15*, 7599–7603. [CrossRef] [PubMed]

64. Saltas, V.; Vallianatos, F. Silicon self-diffusion in Stishovite: Calculations of point defect parameters based on the cBΩ thermodynamic model. *Environ. Sci. Proc.* **2021**, *6*, 6.

65. Chroneos, A.; Bracht, H.; Jiang, C.; Uberuaga, B.P.; Grimes, R.W. Nonlinear stability of E centers in $Si_{1-x}Ge_x$: Electronic structure calculations. *Phys. Rev. B* **2008**, *78*, 195201. [CrossRef]

66. Lumley, S.C.; Grimes, R.W.; Murphy, S.T.; Burr, P.A.; Chroneos, A.; Chard-Tuckey, P.R.; Wenman, M.R. The thermodynamics of hydride precipitation: The importance of entropy, enthalpy and disorder. *Acta Mater.* **2014**, *79*, 351–362. [CrossRef]

67. Wang, H.; Chroneos, A.; Jiang, C.; Schwingenschlögl, U. Special quasirandom structures for gadolinia-doped ceria and related materials. *Phys. Chem. Chem. Phys.* **2012**, *14*, 11737–11742. [CrossRef]

68. Chroneos, A.; Jiang, C.; Grimes, R.W.; Schwingenschlögl, U. Special quasirandom structures for binary/ternary group IV alloys. *Chem. Phys. Lett.* **2010**, *493*, 97–102. [CrossRef]

69. Sarlis, N.V.; Skordas, E.S. Pressure and temperature dependence of the oxygen self-diffusion activation volume in $UO_2$ by a thermodynamical model. *Solid State Ionics* **2016**, *290*, 121–123. [CrossRef]

70. Saltas, V.; Chroneos, A.; Cooper, M.W.D.; Fitzpatrick, M.E.; Vallianatos, F. Investigation of oxygen self-diffusion in $PuO_2$ by combining molecular dynamics with thermodynamic calculations. *RSC Adv.* **2016**, *6*, 103641–103649. [CrossRef]

71. Saltas, V.; Horlait, D.; Sgourou, E.N.; Vallianatos, F.; Chroneos, A. Modelling solid solutions with cluster expansion, special quasirandom structures, and thermodynamic approaches. *Appl. Phys. Rev.* **2017**, *4*, 41301. [CrossRef]

72. Varotsos, P.; Sarlis, N.; Lazaridou, M. Interconnection of defect parameters and stress-induced electric signals in ionic crystals. *Phys. Rev. B* **1999**, *59*, 24–27. [CrossRef]

73. Zhang, B.; Xu, J. Thermodynamic estimation of the compressibility of ferropericlase under high pressure. *AIP Adv.* **2016**, *6*, 115112. [CrossRef]

74. Magomedov, M. Dependence of the parameters of vacancy formation and self-diffusion in a single-component crystal on temperature and pressure. *J. Phys. Chem. Solids* **2022**, *165*, 110653. [CrossRef]

75. Dahlqvist, M.; Rosen, J. The rise of MAX phase alloys—large-scale theoretical screening for the prediction of chemical order and disorder. *Nanoscale* **2022**, *14*, 10958. [CrossRef] [PubMed]

76. Christopoulos, S.R.G.; Kordatos, A.; Cooper, M.W.D.; Fitzpatrick, M.E.; Chroneos, A. Activation volumes of oxygen self-diffusion in fluorite structured oxides. *Mater. Res. Express* **2016**, *3*, 105504. [CrossRef]

77. Sarlis, N.V.; Skordas, E.S. Bulk moduli of $PbS_xSe_{1-x}$, $PbS_xTe_{1-x}$, and $PbSe_xTe_{1-x}$ from the combination of the cBΩ model with the modified Born theory compared to generalized gradient approximation. *Mod. Phys. Lett. B* **2016**, *30*, 1650409. [CrossRef]

78. Varotsos, P.A.; Sarlis, N.V.; Skordas, E.S. Thermodynamics of point defects in solids and relation with the bulk properties: Recent results. *Crystals* **2022**, *12*, 686. [CrossRef]

79. Lafaye, P.; Toffolon-Masclet, C.; Crivello, J.C.; Joubert, J.M. Experimental study, first-principles calculation and thermodynamic modelling of the Cr-Fe-Nb-Sn-Zr quinary system for application as cladding materials in nuclear reactors. *J. Nucl. Mater.* **2021**, *544*, 152692. [CrossRef]

80. Sarlis, N.V.; Skordas, E.S. Interconnection of a thermodynamical model for point defect parameters in solids with the dynamical theory of diffusion. *Solid State Ionics* **2019**, *335*, 82–85. [CrossRef]

81. Saltas, V.; Chroneos, A.; Vallianatos, F. Mg diffusion in Si on a thermodynamic basis. *J. Mater. Sci. Mater. Electron.* **2018**, *29*, 12022–12027. [CrossRef]

82. Kumar, V.; Di Stefano, D.; Rignanese, G.M.; Gonze, X. Li diffusion in Si and LiSi: Nuclear quantum effects and anharmonicity. *J. Chem. Phys.* **2020**, *152*, 244101. [CrossRef] [PubMed]

83. Jiang, B.; Bridges, C.A.; Unocic, R.R.; Pitike, K.C.; Cooper, V.R.; Zhang, Y.P.; Lin, D.Y.; Page, K. Probing the local site disorder and distortion in pyrochlore high-entropy oxides. *J. Am. Chem. Soc.* **2021**, *143*, 4193–4204. [CrossRef] [PubMed]

84. Vovk, R.V.; Obolenskii, M.A.; Zavgorodniy, A.A.; Goulatis, I.L.; Beleskii, V.I.; Chroneos, A. Structural relaxation, metal to insulator transition and pseudo-gap in oxygen deficient $HoBa_2Cu_3O_{7-\delta}$ single crystals. *Physica C* **2009**, *469*, 203–206. [CrossRef]

85. Vovk, R.V.; Vovk, N.R.; Shekhovtsov, O.V.; Goulatis, I.L.; Chroneos, A. c-axis hopping conductivity in heavily Pr-doped YBCO single crystals. *Semicond. Sci. Technol.* **2013**, *26*, 085017. [CrossRef]

86. Rushton, M.J.D.; Chroneos, A.; Skinner, S.J.; Kilner, J.A.; Grimes, R.W. Effect of strain on the oxygen diffusion in yttria and gadolinia co-doped ceria. *Solid State Ionics* **2013**, *230*, 37–42. [CrossRef]

87. Rushton, M.J.D.; Chroneos, A. Impact of uniaxial strain and doping on oxygen diffusion in $CeO_2$. *Sci. Rep.* **2014**, *4*, 6068. [CrossRef]

88. Chroneos, A.; Sgourou, E.N.; Londos, C.A.; Schwingenschlögl, U. Oxygen defect processes in silicon and silicon germanium. *Appl. Phys. Rev.* **2015**, *2*, 021306. [CrossRef]

89. Zhu, J.; Vasilopoulou, M.; Davazoglou, D.; Kennou, S.; Chroneos, A.; Schwingenschlögl, U. Intrinsic defects and H doping in $WO_3$. *Sci. Rep.* **2017**, *7*, 40882. [CrossRef]

90. Jiang, C.; Chroneos, A. Ab initio modelling of MAX phase solid solutions using the special quasirandom structure approach. *Phys. Chem. Chem. Phys.* **2018**, *20*, 1173–1180. [CrossRef]

91. Ewing, R.C. Nuclear waste forms for actinides. *Proc. Natl. Acad. Sci. USA* **1999**, *96*, 3432–3439. [CrossRef]

92. Sickafus, K.E.; Minervini, L.; Grimes, R.W.; Valdez, J.A.; Ishimaru, M.; Li, F.; McClellan, K.J.; Hartmann, T. Radiation tolerance of complex oxides. *Science* **2000**, *289*, 748–751. [CrossRef] [PubMed]

93. Grimes, R.W.; Konings, R.J.M.; Edwards, L. Greater tolerance for nuclear materials. *Nat. Mater.* **2008**, *7*, 683–685. [CrossRef] [PubMed]

94. Grimes, R.W.; Nuttal, W.J. Generating the option of a two-stage nuclear renaissance. *Science* **2010**, *329*, 799–803. [CrossRef] [PubMed]

95. Armaroli, N.; Balzani, V. Towards an electricity-powered world. *Energy Environ. Sci.* **2011**, *4*, 3193–3322. [CrossRef]

96. Garcia-Barriocanal, J.; Rivera-Calzada, A.; Varela, M.; Sefrioui, Z.; Iborra, E.; Leon, C.; Pennycook, S.J.; Santamaria, J. Colossal ionic conductivity at interfaces of epitaxial $ZrO_2$:$Y_2O_3$/$SrTiO_3$ heterostructures. *Science* **2008**, *321*, 676–680. [CrossRef]

97. Kilner, J.A. Ionic conductors: Feel the strain. *Nat. Mater.* **2008**, *7*, 838. [CrossRef]

98. Guo, X. Comment on "Colossal ionic conductivity at interfaces of epitaxial $ZrO_2$:$Y_2O_3$/$SrTiO_3$ heterostructures". *Science* **2009**, *324*, 5926. [CrossRef]

99. Schichtel, N.; Korte, C.; Hesse, D.; Janek, J. Elastic strain at interfaces and its influence on ionic conductivity in nanoscaled solid electrolyte thin films- theoretical considerations and experimental studies. *Phys. Chem. Chem. Phys.* **2009**, *11*, 3043–3048. [CrossRef]

100. Kushima, A.; Yildiz, B. Oxygen ion diffusivity in strained yttria stabilized zirconia: Where is the fastest strain? *J. Mater. Chem.* **2010**, *20*, 4809–4819. [CrossRef]

101. Chroneos, A.; Yildiz, B.; Tarancón, A.; Parfitt, D.; Kilner, J.A. Oxygen diffusion in solid oxide fuel cell cathode and electrolyte materials: Mechanistic insights from atomistic simulations. *Energy Environ. Sci.* **2011**, *4*, 2774–2789. [CrossRef]

102. Cavallaro, A.; Burriel, M.; Roqueta, J.; Apostolidis, A.; Bernardi, A.; Tarancón, A.; Srinivasan, R.; Cook, S.N.; Fraser, H.L.; Kilner, J.A.; et al. Electronic nature of the enhanced conductivity in YSZ-STO multilayers deposited by PLD. *Solid State Ionics* **2010**, *181*, 592–601. [CrossRef]

103. Pennycook, T.J.; Beck, M.J.; Varga, K.; Varela, M.; Pennycook, S.J.; Pantelides, S.T. Origin of colossal ionic conductivity in oxide multilayers: Interface induced sublattice disorder. *Phys. Rev. Lett.* **2010**, *104*, 115901. [CrossRef] [PubMed]

104. De Souza, R.A.; Ramadan, A.; Hörner, S. Modifying the barriers for oxygen-vacancy migration in fluorite-structured $CeO_2$ electrolytes through strain; A computer simulation study. *Energy Environ. Sci.* **2012**, *5*, 5445–5453. [CrossRef]

105. Korte, C.; Schichtel, N.; Hesse, D.; Janek, J. Influence of interface structure on mass transport in phase boundaries between different ionic materials: Experimental studies and formal considerations. *Monatsh. Chem.* **2009**, *140*, 1069–1080. [CrossRef]

106. Chiabrera, F.; Garbayo, I.; Lopez-Conesa, L.; Martin, G.; Ruiz-Caridad, A.; Walls, M.; Ruiz-Gonzalez, L.; Kordatos, A.; Nunez, M.; Morata, A.; et al. Engineering transport in manganites by tuning local nonstoichiometry in grain boundaries. *Adv. Mater.* **2019**, *31*, 1805360. [CrossRef]

107. Acosta, M.; Baiutti, F.; Tarancon, A.; MacManus-Driscoll, J.L. Nanostructured materials and interfaces for advanced ionic electronic conducting oxides. *Adv. Mater. Interfaces* **2019**, *6*, 1–15. [CrossRef]

108. Lee, D.; Gao, X.; Sun, L.; Jee, Y.; Poplawsky, J.; Farmer, T.O.; Fan, L.; Guo, E.-J.; Lu, Q.; Heller, W.T.; et al. Colossal oxygen vacancy formation at a fluorite-bixbyite interface. *Nat. Commun.* **2021**, *11*, 1371. [CrossRef]

109. Baiutti, F.; Chiabrera, F.; Acosta, M.; Diercks, D.; Parfitt, D.; Santiso, J.; Wang, X.; Cavallaro, A.; Morata, A.; Wang, H.; et al. A high-entropy manganite in an ordered nanocomposite for long-term application in solid oxide cells. *Nat. Commun.* **2021**, *12*, 2660. [CrossRef]

110. Kuganathan, N.; Baiutti, F.; Tarancon, A.; Fleig, J.; Chroneos, A. Defects energetics in the $SrTiO_3$-$LaCrO_3$ system. *Solid State Ionics* **2021**, *361*, 115570. [CrossRef]

111. Navickas, E.; Huber, T.M.; Chen, Y.; Hetaba, W.; Holzlechner, G.; Rupp, G.; Stöger-Pollach, M.; Friedbacher, G.; Hutter, H.; Yildiz, B.; et al. Fast oxygen exchange and diffusion kinetics of grain boundaries in Sr-doped $LaMnO_3$ thin films. *Phys. Chem. Chem. Phys.* **2015**, *17*, 7659–7669. [CrossRef]

112. Saranya, A.M.; Pla, D.; Morata, A.; Cavallaro, A.; Canales-Vazquez, J.; Kilner, J.A.; Burriel, M.; Tarancon, A. Engineering mixed ionic electronic conduction in $La_{0.8}Sr_{0.2}MnO_{3+\delta}$ nanostructures through fast grain boundary oxygen diffusivity. *Adv. Energy Mater.* **2015**, *5*, 1500377. [CrossRef]

113. Saranya, A.M.; Morata, A.; Pla, D.; Burriel, M.; Chiabrera, F.; Garbayo, I.; Hornes, A.; Kilner, J.A.; Tarancon, A. Unveiling the outstanding oxygen mass transport properties of Mn-rich perovskites in grain boundary-dominated $La_{0.8}Sr_{0.2}(Mn_{1-x}Co_x)_{0.85}O_{3\pm\delta}$ nanostructures. *Chem. Mater.* **2018**, *30*, 5621–5629. [CrossRef]

114. Sun, L.; Marrocchelli, D.; Yildiz, B. Edge dislocation slows down oxide ion diffusion in doped $CeO_2$ by segregation of charged defects. *Nat. Commun.* **2015**, *6*, 6294. [CrossRef] [PubMed]

115. Marrocchelli, D.; Sun, L.; Yildiz, B. Dislocation in $SrTiO_3$: Easy to reduce but not so fast for oxygen transport. *J. Am. Chem. Soc.* **2015**, *137*, 4735–4748. [CrossRef] [PubMed]

116. Solovjov, A.L.; Tkachenko, M.A.; Vovk, R.V.; Chroneos, A. Fluctuation conductivity and pseudogap in $HoBa_2Cu_3O_{7-\delta}$ single crystals under pressure with transport current flowing under an angle $45°$ to the twin boundaries. *Physica C* **2014**, *501*, 24–31. [CrossRef]

117. Vovk, R.V.; Nazyrov, Z.F.; Obolenskii, M.A.; Goulatis, I.L.; Chroneos, A.; Simoes, V.M.P. Phase separation in oxygen deficient $HoBa_2Cu_3O_{7-\delta}$ single crystals: Effect of pressure and twin boundaries. *Philos. Mag.* **2011**, *91*, 2291–2302. [CrossRef]

118. Vovk, R.V.; Obolenskii, M.A.; Zavgorodniy, A.A.; Bondarenko, A.V.; Goulatis, I.L.; Samoilov, A.V.; Chroneos, A. Effect of high pressure on the fluctuation conductivity and the charge transfer of $YBa_2Cu_3O_{7-\delta}$ single crystals. *J. Alloys Compds.* **2008**, *453*, 69–74. [CrossRef]

119. Vovk, R.V.; Obolenskii, M.A.; Nazyrov, Z.F.; Goulatis, I.L.; Chroneos, A.; Simoes, V.M.P. Electro-transport and structure of 1-2-3 HTSC single crystals with different plane defect topologies. *J. Mater. Sci. Mater. Electron.* **2012**, *23*, 1255–1259. [CrossRef]

120. Solovjov, A.L.; Petrenko, E.V.; Omelchenko, L.V.; Vovk, R.V.; Goulatis, I.L.; Chroneos, A. Effect of annealing on a pseudogap state in untwinned $YBa_2Cu_3O_{7-\delta}$ single crystals. *Sci. Rep.* **2019**, *9*, 9274. [CrossRef]

121. Seymour, I.D.; Chroneos, A.; Kilner, J.A.; Grimes, R.W. Defect processes in orthorhombic $LnBaCo_2O_{5.5}$ double perovskites. *Phys. Chem. Chem. Phys.* **2011**, *13*, 15305–15310. [CrossRef]

122. Yildiz, B. "Stretching" the energy landscape of oxides- Effects on eletrocatalysis and diffusion. *MRS Bull.* **2014**, *39*, 147–156. [CrossRef]

123. Ma, W.; Kim, J.J.; Tsvetkov, N.; Daio, T.; Kuru, Y.; Cai, Z.; Chen, Y.; Sasaki, K.; Tuller, H.L.; Yildiz, B. Vertically aligned nanocomposite $La_{0.8}Sr_{0.2}CoO_3/(La_{0.5}Sr_{0.5})_2CoO_4$ cathodes—electronic structure, surface chemistry and oxygen reduction kinetics. *J. Mater. Chem. A* **2015**, *3*, 207–219. [CrossRef]

124. Jay, E.E.; Rushton, M.J.D.; Chroneos, A.; Grimes, R.W.; Kilner, J.A. Genetics of superionic conductivity in lithium lanthanum titanates. *Phys. Chem. Chem. Phys.* **2015**, *17*, 178–183. [CrossRef]

125. Kuganathan, N.; Rushton, M.J.D.; Grimes, R.W.; Kilner, J.A.; Gkanas, E.I.; Chroneos, A. Self-diffusion in garnet-type $Li_7La_3Zr_2O_{12}$ solid electrolytes. *Sci. Rep.* **2021**, *11*, 451. [CrossRef] [PubMed]

126. Kuganathan, N.; Chroneos, A. Defects, diffusion, dopants and encapsulation of Na in NaZr$_2$(PO$_4$)$_3$. *Materialia* **2021**, *16*, 101039. [CrossRef]

127. Kuganathan, N.; Chroneos, A. Defects, dopants and sodium mobility in Na$_2$MnSiO$_4$. *Sci. Rep.* **2018**, *8*, 14669. [CrossRef] [PubMed]

128. Tsuruaka, T.; Tsujita, T.; Su, J.; Nishitani, Y.; Hamamura, T.; Inatomi, Y.; Nakura, K.; Terabe, K. Fabrication of a magnesium-ion conducting magnesium phosphate electrolyte film using atomic layer deposition. *Jpn. J. Appl. Phys.* **2020**, *59*, SIIG08. [CrossRef]

129. Kuganathan, N.; Davazoglou, K.; Chroneos, A. Computer modelling investigation of MgV$_2$O$_4$ for Mg-ion batteries. *J. Appl. Phys.* **2020**, *127*, 035106. [CrossRef]

130. Hasa, I.; Mariyappan, S.; Saurel, D.; Adelhelm, P.; Koposov, A.Y.; Masquelier, C.; Croguennec, L.; Casas-Cabanas, M. Challenges of today for Na-based batteries of the future: From materials to cell metrics. *J. Power Sources* **2021**, *482*, 228872. [CrossRef]

131. Liu, R.Q.; Kumar, A.; Chen, Z.Z.; Agrawal, A.; Sundararaghavan, V.; Choudhary, A. A predictive machine learning approach for microstructure optimization and materials design. *Sci. Rep.* **2015**, *5*, 22552. [CrossRef]

132. Bouchard, P.J. Validated residual stress profiles for fracture assessments of stainless steel pipe girth welds. *Int. J. Press. Vessels Pip.* **2007**, *84*, 195–222. [CrossRef]

133. Wei, J.; Chu, X.; Sun, X.Y.; Xu, K.; Deng, H.X.; Chen, J.G.; Wei, Z.M.; Lei, M. Machine learning in materials science. *InfoMat* **2019**, *1*, 338–358. [CrossRef]

134. Gubernatis, J.E.; Lookman, T. Machine learning in materials design and discovery: Examples from the present and suggestions for the future. *Phys. Rev. Mater.* **2018**, *2*, 12301–123016. [CrossRef]

135. Mathew, J.; Parfitt, D.; Wilford, K.; Riddle, N.; Alamaniotis, M.; Chroneos, A.; Fitzpatrick, M.E. Reactor pressure vessel embrittlement: Insights from neural network modelling. *J. Nucl. Mater.* **2018**, *502*, 311–322. [CrossRef]

136. Pace, J.V.; Rosseel, T.M.; Wang, J.A. US NRC Embrittlement Data Base. 1999. Available online: http://www.osti.gov/scitech/biblio/14353 (accessed on 25 August 2022).

137. Rosenblatt, F. The perceptron: A probabilistic model for information storage and organization in the brain. *Psychol. Rev.* **1958**, *65*, 386–408. [CrossRef] [PubMed]

138. Li, Y.; Lei, G.; Bramerdorfer, G.; Peng, S.; Sun, X.; Zhu, J. Machine learning for design optimization of electromagnetic devices: Recent developments and future directions. *Appl. Sci.* **2021**, *11*, 1627. [CrossRef]

139. Alamaniotis, M.; Mathew, J.; Chroneos, A.; Fitzpatrick, M.; Tsoukalas, L. Probabilistic kernel machines for predictive monitoring of weld residual stress in energy systems. *Eng. Appl. Artif. Intell.* **2018**, *71*, 138–154. [CrossRef]

140. Odette, G.R.; Lucas, G.E.; Klingensmith, D.; Wirth, B.D.; Gragg, D. The Effects of Composition and Heat Treatment on Hardening and Embrittlement of Reactor Pressure Vessel Steels. [Internet], NUREG/CR-6778; 2003. Available online: http://www.nrc.gov/docs/ML0317/ML031700122.pdf (accessed on 25 August 2022).

141. Mathew, J.; Griffin, J.; Alamaniotis, M.; Kanarachos, S.; Fitzpatrick, M.E. Prediction of welding residual stresses using machine learning: Comparison between neural networks and neuro-fuzzy systems. *Appl. Soft Comp.* **2018**, *70*, 131–146. [CrossRef]